Author's Accepted Manuscript

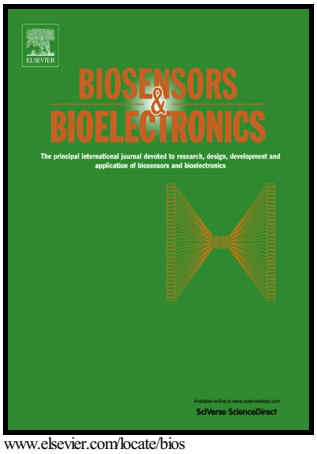

www.elsevier.com/locate/bios

Three-dimensional graphene biointerface with extremely high sensitivity to single cancer cell monitoring

Xiahua Wang, Aiping Liu, Yun Xing, Hongwei Duan, Weizhong Xu, Qi Zhou, Huaping Wu, Cen Chen, Benyong Chen

PII: S0956-5663(18)30020-4
DOI: https://doi.org/10.1016/j.bios.2018.01.012
Reference: BIOS10205

To appear in: *Biosensors and Bioelectronic*

Received date: 20 November 2017
Revised date: 2 January 2018
Accepted date: 8 January 2018

Cite this article as: Xiahua Wang, Aiping Liu, Yun Xing, Hongwei Duan, Weizhong Xu, Qi Zhou, Huaping Wu, Cen Chen and Benyong Chen, Three-dimensional graphene biointerface with extremely high sensitivity to single cancer cell monitoring, *Biosensors and Bioelectronic,* https://doi.org/10.1016/j.bios.2018.01.012

This is a PDF file of an unedited manuscript that has been accepted for publication. As a service to our customers we are providing this early version of the manuscript. The manuscript will undergo copyediting, typesetting, and review of the resulting galley proof before it is published in its final citable form. Please note that during the production process errors may be discovered which could affect the content, and all legal disclaimers that apply to the journal pertain.

ACCEPTED MANUSCRIPT

Three-dimensional graphene biointerface with extremely high sensitivity to single cancer cell monitoring

Xiahua Wang [a], Aiping Liu [a,b,*], Yun Xing [a], Hongwei Duan [c], Weizhong Xu [a], Qi Zhou [a], Huaping Wu [d,e], Cen Chen [f], Benyong Chen [a,*]

[a] *Nanometer Measurement Laboratory, Center for Optoelectronics Materials and Devices, Zhejiang Sci-Tech University, Hangzhou, 310018, China*

[b] *State Key Laboratory of Structural Analysis for Industrial Equipment, Dalian University of Technology, Dalian 116024, China*

[c] *School of Chemical and Biomedical Engineering, Nanyang Technological University, 637457, Singapore*

[d] *Key Laboratory of E&M (Zhejiang University of Technology), Ministry of Education & Zhejiang Province, Hangzhou 310014, China*

[e] *State Key Laboratory for Strength and Vibration of Mechanical Structures, Xi'an Jiaotong University, Xi'an 710049, China*

[f] *College of Life Sciences, Zhejiang Sci-Tech University, Hangzhou 310018, China*

Corresponding author. Center for Optoelectronics Materials and Devices, Zhejiang Sci-Tech University, No. 928, Street 2, Hangzhou 310018. Tel. +86-571-86843574. E-mail address: liuaiping1979@gmail.com, chenby@zstu.edu.cn.

Accepted manuscript

ACCEPTED MANUSCRIPT

ABSTRACT: We developed a three-dimensional biointerface of graphene-based electrical impedance sensor for metastatic cancer diagnosis at single-cell resolution. Compared with traditional impedance sensor with two-dimensional interface, the graphene biointerface mimiced the topography and somatotype features of cancer cells, achieving more comprehensive and thorough single cell signals in the three-dimensional space. At the nodes of physiological behaviour change of single cell, namely cell capture, adhesion, migration and proliferation, the collected electrical signals from graphene biointerface were about two times stronger than those from the two-dimensional gold interface due to the substantial increase in contact area and significant improvement of topographical interaction between cells and graphene electrode. Simultaneous CCD recording and electrical signal extraction from the entrapped single cell on the graphene biointerface enabled to investigate multidimensional cell-electrode interactions and predict cancerous stage and pathology.

Keywords: Three-dimensional graphene biointerface, electrical cell-substrate impedance sensor (ECIS), topographical interaction, metastatic cancer diagnosis, single cell capture

Accepted manuscript

ACCEPTED MANUSCRIPT

1. Introduction

The death induced by the cancer is given great attention all the time. Usually, cancer cells differ from healthy cells in adhesion, migration, proliferation and maturation (Ertel et al., 2006; Meadows et al., 2008; Sell, 2010; Nguyen et al., 2013), which might lead to changes in electrical activities of the cells (Han et al., 2007). Over the past few years, many label-free non-invasive devices, such as field-effect transistor (Ang et al., 2011), electric impedance meter (Babahosseini et al., 2016) and electrical cell-substrate impedance sensor (ECIS) (Hong et al., 2011), have been used to assess cell status and provide real-time cell behavior information. Among them, the electrical cell-substrate impedance sensing technology is a powerful biophysical method to monitor many cellular events (including adhesion, growth, metastasis, migration, electroporation, wound healing and death) (Giaever and Keese, 1993; Xiao et al., 2002; Keese et al., 2004; Valastyan and Weinberg, 2011; Sperber et al., 2015; Guo and Zhu, 2016; Xu et al., 2016), and reveal information about cell-electrode interactions (Liu et al., 2014), single cell movements (Sun and Morgan, 2010) and cell-cell communication (Moodley et al., 2011) by measuring the cellular impedance changes at different biological processes on the artificial electrode interfaces (Wang et al., 2008; Chang et al., 2011). Nevertheless, the contact between electrode materials and cell membranes in this system is usually constrained on the transverse surface. The collected electrical signals can only reflect cell movements in the horizontal direction and the extension in the vertical direction is unreachable.

To overcome these limitations of classically planar, plate-like electrodes, more sophisticated electrode designs, such as single or aggregated carbon nanotube array electrodes (Wang et al., 2006; Abdolahad et al., 2012; Abdolahad et al., 2013), nanowire array electrodes (Yang et al., 2013; Abdolahad et al., 2014; Abiri et al., 2015) and various graphene-based electrodes (Hess et al., 2013) are proposed and developed for fast, efficient

Accepted manuscript

ACCEPTED MANUSCRIPT

and specific diagnosis of cancer cells in the ECIS system. The surface textures of these electrodes are more biomimetic, which significantly enhance the binding strength and interfacial interactions between electrodes and cells, improving both the transduced signals and the electrical stimulation efficiency (Blau, 2013). However, the electrical impedance sensitivity for the single cell in these interfaces is limited due to the failure in the identification of multiple morphologies and characteristics of single cancer cell. The faint signal from the single cell is easy to be merged into the averaged response of a cell population (Levsky and Singer, 2003). Based on this, three-dimensional (3D) biointerface might be more effective for cell-related biological studies (Liu and Wang, 2014; Cai et al., 2017) because 3D biointerface could conduct cell growth in a manageable and accurate way (Nikkhah et al., 2012), resulting in the enhancement of cell attachment (Liu et al., 2013; Duy et al., 2015), the promotion of cell interconnection to outside (Kim et al., 2007; Park et al., 2012), and the strengthening of cell response to external stimulus (Keefer et al., 2008; Robinson et al., 2012). If the 3D biointerface is merged into a microfluidic system (Khademhosseini et al., 2005; Qian et al., 2015; Wu et al., 2017), it is possible to obtain an ideal interface for highly efficient and sustained detection of single cancer cell behavior.

Herein we demonstrated the fabrication of 3D micro/nano structured graphene interface and their outstanding capability of impedance signal sensing in single cancer cell. The 3D microgroove conformation fabricated by the lithography technology was inspired by the shape and size of cancer cells as well as their surface nanostructures. The choice of graphene as electrode material is unequivocal because of its large specific surface area, high carrier mobility, excellent electrochemical performance and biocompatibility (Liu et al., 2016; Zhao et al., 2017), demonstrating its great potential in cell-related studies (Hess et al., 2011; Feng et al., 2013; Kuzum et al., 2014; Li et al., 2015). However, the capacity of 3D graphene biointerface as the sensing electrode for single cell detection has not been explored. Our

Accepted manuscript

ACCEPTED MANUSCRIPT

results verified that the admirable biointerface of graphene modified microgroove electrodes could greatly improve the sensing sensitivity of electrical impedance signals of cancer cells at multiple frequencies when compared to the classic 2D gold electrodes. Therefore, this study is very significative in guiding functional design of bio-inspired hierarchical interfaces for cancer cell diagnosis.

2. Experimental section

2.1. Design of 3D graphene biointerface on the microfluidic chip

Fig. 1(a) showed the panoptic design of microfluidic chip, which comprised three main parts, namely integrated electrode arrays, a poly-dimethylsiloxane (PDMS) channel and a PDMS lid (Fig. S1). The integrated electrode arrays consisted of the 3D graphene modified photoresist-microgroove electrode arrays (GMEAs) with 2D gold bottom electrode. According to the injection direction of cell fluid, the GMEAs on both sides of the central reference electrode (2 cm×2 mm) were regarded as the working electrodes (with cells) and the counter electrodes (without cell), respectively (Fig. 1b). Two sizes of gold bottom electrodes (Fig. 1c) were first designed for electrical signal transmission of single cell (25×20 μm^2, Fig. 1d) and double cells (45×25 μm^2). In order to increase the multidimensional contact between graphene films and cell membranes, the 3D GMEAs were designed to be hollow semi-cylindrical (Fig. 1c) for better matching with the size and shape of the single (18×17×30 μm^3, Fig. 1d) or double breast cancer cells (30×21×30 μm^3). To prevent the cells over-accumulation in trapping posts and guarantee cell capture efficiency, a 5-μm slit in the centerline position between two grooves was reserved to allow the solution flowing (Eyer et al., 2013). The PDMS lid fabricated through standard micro-molding processes (Jo et al., 2000) (Fig. S1) could be partially opened for straightforward observation of cell behaviors.

Accepted manuscript

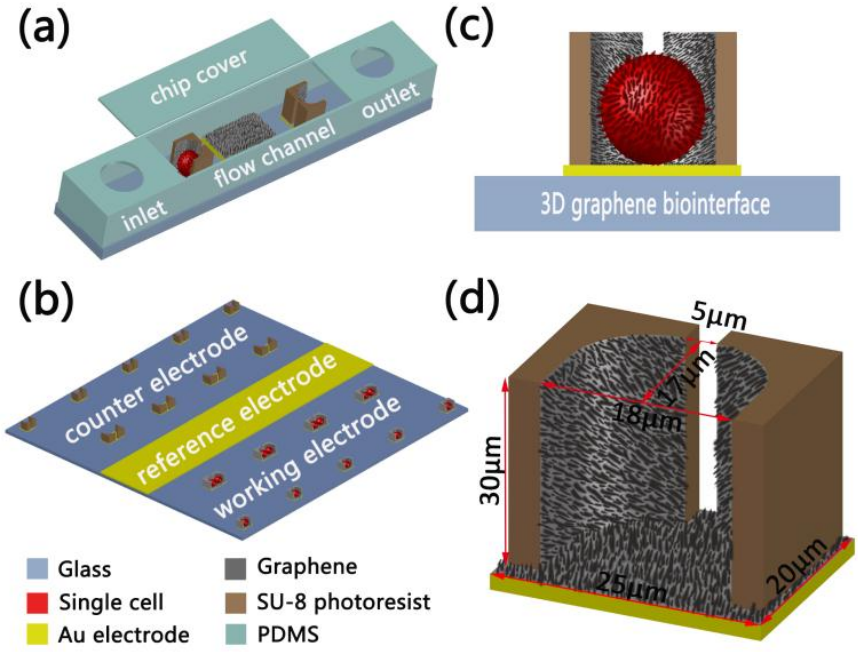

Fig. 1.

2.2. Fabrication of 3D graphene biointerface on the microfluidic chip

The 2D gold bottom electrode arrays (PGEAs) were firstly formed on the glass substrate (2×2 cm^2) through a lift-off process (see more details in Fig. S2). Then, a 25-μm-thick negative photoresist (Ruicai, SU-8) was spin-coated on this substrate (Fig. 2a) and subsequently patterned and developed by the lithography technology (Fig. 2b-2e). Then the 3D photoresist microgrooves were hydrophilizated by O_2 plasma treatment (KeYou, China) with 20 W power for 1 min (Fig. 2f) and incubated in 1 mL of PDDA aqueous solution (Sigma Aldrich, 20 wt%) at 35°C for 1 h (Fig. 2g). After a 300μL of 1mg/mL graphene oxide (GO, prepared by the Hummer's method (Marcano et al., 2010)) solution was titrated onto the modified hydrophilic surfaces and incubated at 40°C for 12 h (Fig. 2h), the GO layer was reduced to graphene under hydrazine hydrate vapour at 80°C for 10 h (Fig. 2i), forming 3D microgrooves with multi-layered graphene covered. An annealing treatment at 200°C in a dry N_2 stream for 2 h was helpful for the improvement of ohmic contact between gold and graphene. Finally, the continuous graphene film was cut into pieces according to the designed

Accepted manuscript

sensing units by a laser dicing with a 0.8 J/cm^2 energy density (Hong and Jang, 2012) to avoid the interference of electrical signals in every independent unit (Fig. 2j). After the H-shaped PDMS channel and PDMS lid were manually bonded on the substrate with integrated electrode arrays, the entire microfluidic chip was achieved.

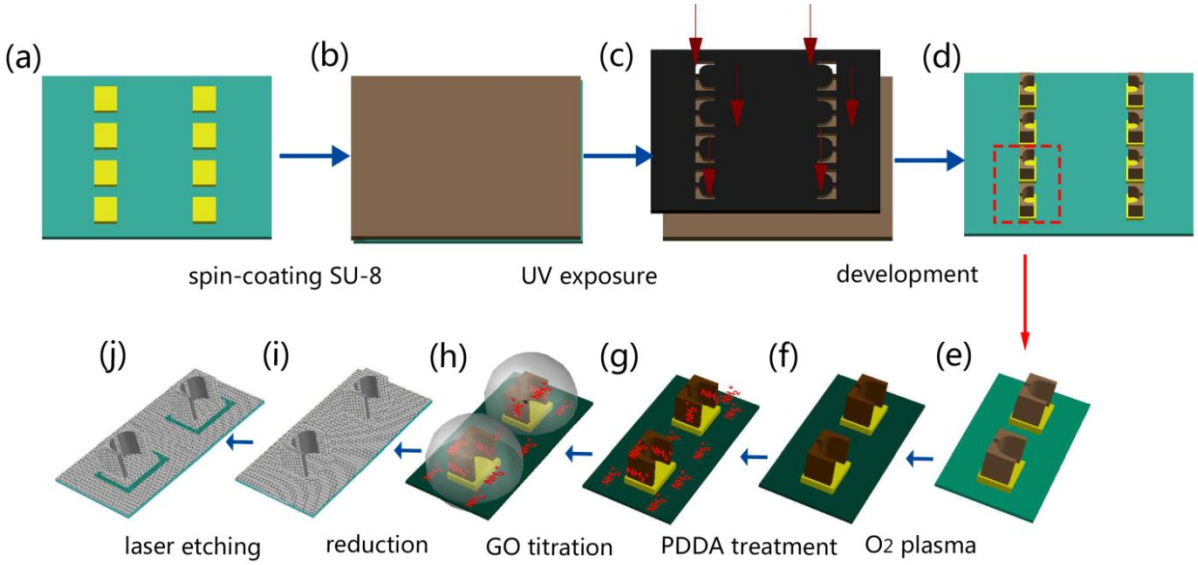

Fig. 2.

2.3. Cell culture and seeding

Breast cancer cells (MCF-7 and MDA-MB-231) were obtained from the National Infrastructure of Cell Line Resource and incubated in Dulbecco's modified Eagle's medium (DMEM/High Glucose, HyClone, Logan, UT) supplemented with 10 % fetal bovine serum (FBS, HyClone, Logan, UT) and 1 % penicillin-streptomycin solution (HyClone, Logan, UT) for 2 to 3 days (37°C, 5% CO_2, 95 % humidity environment). The phosphate-buffered solution (PBS, pH=7.4, 1mg/mL, Solarbio Technology Co., Ltd, Beijing, China) added with calcium and magnesium was used to wash cells. Then the cells were detached from culture flasks by treatment with trypsin-EDTA (Solarbio Technology Co., Ltd, Beijing, China), centrifuged at 1000 rpm for 10 min and seeded in the culture flasks with a concentration of 10^6 cells/mL for further incubation and experiment.

Accepted manuscript

ACCEPTED MANUSCRIPT

2.4. Measurement and characterization

The morphologies of graphene modified microgrooves were recorded on a field emission scanning electron microscope (FESEM, Hitachi S4800), a shape measuring laser microscope system (KEYENCE VK-X100, Japan) and an atomic force microscope (AFM, Bruker, Germany). Raman spectra were recorded on a Thermo Fisher DXR Raman spectrometer using a He-Ne laser (λ=632.8nm). The electrical conductivity of graphene films were measured using a standard four-point-probe system by a source meter (Keithley 2400, USA). The electrochemical behaviors of the $Fe_3(CN)_6^{3-/4-}$ redox couple at graphene films were investigated in the 2.5 mM $K_3Fe(CN)_6$ and 0.1 M KCl mixed solution on the CHI660B electrochemical workstation (Shanghai Chenhua Instrument Co., China) in a three-electrode system (the GMEAs as the working electrode, Ag/AgCl electrode as the reference electrode and Pt piece as the counter electrode). The electrical impedance signals of cells captured by the 3D graphene modified electrode on the microfluidic chip were recorded in a test system for microfluidic chip with an impedance spectroscope (HF2IS, Zurich, see Fig. S3 and Fig. S4). Two different modes (frequency domain and time domain) were used in the electrical impedance measurement.

3. Results and discussion

3.1. Characterizations of 3D graphene biointerface

Fig. 3a shows a photograph of designed microfluidic chip (2×2 cm^2). The integrated electrode arrays are connected to the corresponding visible large gold electrodes (2×2 mm^2) around the chip for the integration with printed circuit board (PCB). The magnified microscope image of microchannel presents the cell capture regions for single cell and double cells (Fig. 3b). The height of hollow semicylinder is about 30 μm (Fig. 3c), which is helpful for enlarging contact area between captured cells and GMEAs in the vertical direction. After

Accepted manuscript

graphene modification on the microgrooves (Fig. 3d), the rough edges are clearly visible (Fig. 3e). The side wall of the microgroove is densely packed by graphene sheets (Fig. 3f) with a nanostructured surface (Fig. 3g). The hierarchical biointerface has the potential capability of interacting with cellular pseudopods, enhancing cell attachment and promoting cell sensing to external signals. After the continuous graphene films were laser etched (Fig. 3h), the single capture unit separated by the exposed glass substrate (Fig. 3i) indicates that the laser etching is very thorough without any residues. This would reduce the mutual interference of electrical signals of each unit. The successful modification and reduction of graphene sheets on the microgrooves were further confirmed by Raman, conductivity and electrochemical measurements (Fig. S5, see more discussion in Supporting Information). The excellent and stable conductivity and electrochemical activity of graphene film indicate its tremendous superiority as an electrode material.

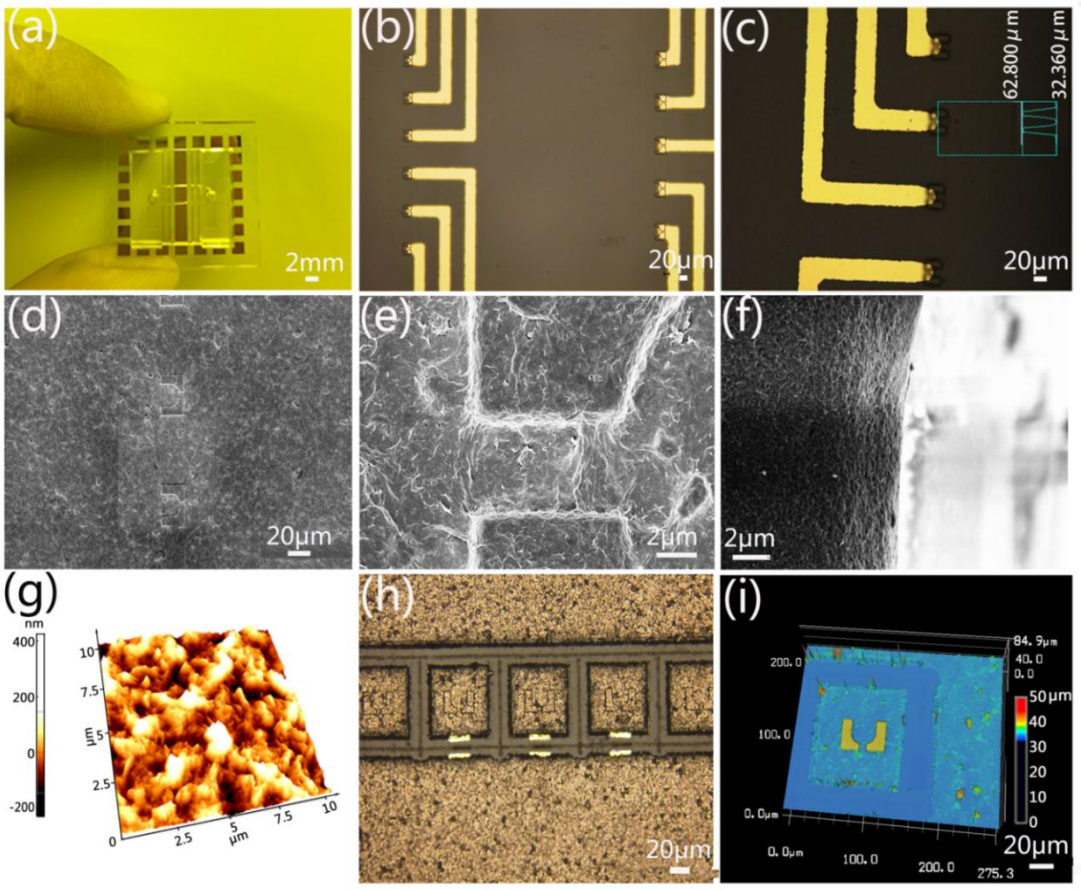

Fig. 3.

ACCEPTED MANUSCRIPT

3.2. Capture and morphology of the cells on 3D graphene biointerface

After the cells were trapped in the corresponding microgrooves of 2D gold interfaces (Fig. 4a-4b) and 3D graphene biointerfaces (Fig. 4c-4d), their morphologies were observed by a laser microscope equipped with a CCD. The cells captured by the graphene biointerfaces contact with the surrounding graphene electrode more closely than those captured by the gold interfaces due to the increased circumambient roughness and conductivity after modifying graphene on the photoresist microgrooves. Furthermore, the single cell (or double cells) presents packaged (Fig. 4e or Fig. 4f) and squeezed (Fig. 4g or Fig. 4h) states, revealing the improved interaction between the cells and graphene biointerfaces on multiple dimensions by the protruded filopodia of cells. Therefore, it could be deduced that the breast cancer cells would be more willing to attach the rough and conductive graphene surface rather than the smooth gold surface because of the orographic interactions that happen through the nanotexture-induced matching effect and the microgroove-induced 3D trap effect (Li et al., 2015), which might be essential for the ultrahigh sensing capacity.

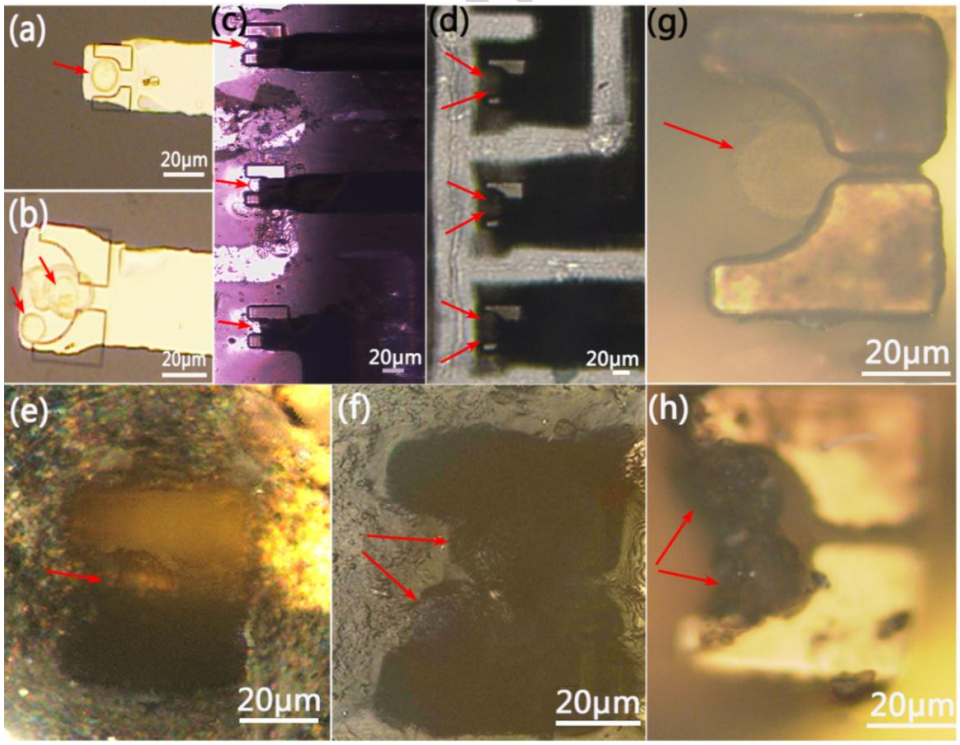

Fig. 4.

ACCEPTED MANUSCRIPT

3.3. Cell-electrode interaction in different cell culturing and metastatic progression stages

The cell-induced impedance signal change was investigated by the ECIS technology. The high detection sensitivity of GMEAs is firstly confirmed by measuring the impedance response of different solutions (distilled water, deionized water, PBS, 75 % alcohol, 95 % alcohol and cell culture medium) with same volumes when they are injected into the microfluidic chip through the sampling control system. The clear distinction in the impedance amplitude and phase value is observed in the frequency ranging from 100 Hz to 1M Hz (Fig. S6a). Furthermore, a 30 % increase in the impedance magnitude and phase value is obtained from the GMEAs compared with those obtained from the PGEAs (Fig. S6b), proving the obvious advantage of 3D graphene biointerface in electrical impedance sensing.

In the cell capture, attachment (0-2h), spreading (2-5h) and proliferation (5-9h) periods (Abiri et al., 2015), the changes of impedance magnitude and phase value were achieved after single or double metastatic (MDA-MB-231) or less-metastatic (MCF-7) breast cancer cells were captured and cultivated in the 2D gold interface or 3D graphene biointerface (Fig. S7 and Fig. S8). Besides the electrical signals extraction of cells at different physiological stages, the real-time monitoring of cell morphology was also obtained by the simultaneous CCD recording (Fig. S9). The statistical analysis of the increment in impedance ΔZ (which is the difference between the impedance of latter state and the one of former state, for example, $\Delta Z_{proliferation}=Z_{proliferation}-Z_{spreading}$) obtained at two frequencies of 5k Hz and 10k Hz in the time domain is showed in Fig. 5 (the average value of five results ± standard deviation). At the nodes of cell state change, the ΔZ related to single cell and double cells obtained at the 3D graphene biointerface are about 100% and 50%, respectively, when compared to the 2D gold interface. In addition, the differences in impedance change caused by cancer metastatic progression ($\Delta Z_{MCF-7}-\Delta Z_{MDA-MB-231}$) in single cell and double cells at various seeding stages through using the 3D graphene biointerface are obviously larger than those using the 2D gold

Accepted manuscript

interface (Table S1). These statistical data indicate that the 3D graphene biointerface is extremely sensitive for cell physiological behavior change and cancer metastatic process. The reason might be that the nanotexture-induced matching effect and the microgroove-induced 3D trapping effect (Li et al., 2015) observably enhance the contact area and synergistically topographic interactions between the graphene electrode and cells, which therefore forcefully adjust current penetration into cancer cells. The obvious structure and interface advantage of 3D graphene film in the study of cell carcinogenesis is further proved by the capture and culture experiment of double cells (Fig. S8).

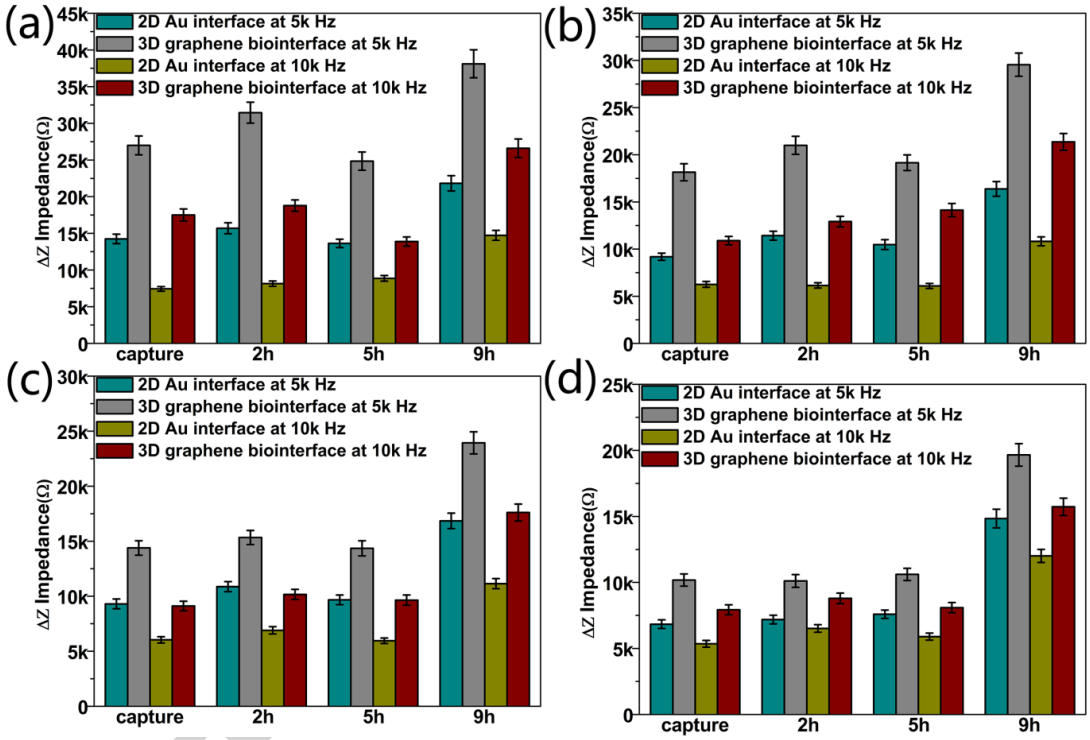

Fig. 5.

4. Theoretical calculation

The electrical equivalent circuit model of the cells seeding on the 2D or 3D interface is further provided for better understanding the cell-electrode interaction. The 2D interface system consists of three main parts, namely the electrode-electrolyte interface, the cell-

ACCEPTED MANUSCRIPT

electrode interaction and solution resistance (Fig. 6a) (Franks et al., 2005). In detail, a typical electric circuit which is constituted by a constant phase element Z_{CPE1} in parallel with a charge transfer resistance R_{ct}, is used to simulate the electrode-electrolyte interface. The impedance of constant phase element, which represents interface capacitance impedance, is defined as $Z_{CPE1} = 1/(j\omega Q)^n$, where ω is the angular frequency, Q is the magnitude of Z_{CPE1}, and n is a constant ($0 \leq n \leq 1$) standing for the inhomogeneity in the surface. The value of R_{sol} is determined by the ion concentration in the solution between the working electrode and the reference electrode. The cell-electrode interaction can be simply modeled by the cell impedance Z_{cell} in parallel with a seal resistance R_{seal}. As well as, the cell impedance Z_{cell} comprises a membrane resistance R_m, shunted by a membrane capacitance C_m (Solly et al., 2004). There are several tens to hundreds of nanometers cleft between the electrode surface and the cell membrane in virtue of the existence of the finite binding force and the cell membrane proteins (Giaever and Keese, 1991). Accordingly, R_{seal} describes the tightness of the cell attaching to the electrode, which gives rise to the extended cleft of electrode surface (Borkholder, 1998). Thus, the entire impedance of the cell-electrode interaction on the 2D gold interface can be defined as (Equation 1)

$$Z_{cell-gold} = R_{sol} + \frac{R_{seal}R_m}{R_m + R_{seal} + j\omega R_m R_{seal} C_m} + \frac{R_{ct}Z_{CPE1}}{R_{ct} + Z_{CPE1}} \quad (1)$$

However, the graphene-electrolyte interface is more complex, which cannot be well modeled by this double layer capacitance structure. Many researchers have corroborated the presence of quantum capacitance in graphene (Fang et al., 2007) and the graphene-electrolyte interface could be regarded as a series ensemble of the quantum capacitance and the double layer capacitance (Xia et al., 2009). Therefore, the graphene-electrolyte interface can be interpreted by an intensive double layer capacitance theory. More concretely, another constant phase element C_{PE2} and a leakage resistance R_L are added to the primary circuit

Accepted manuscript

ACCEPTED MANUSCRIPT

model of the gold interface (Du et al., 2015). As illustrated in Fig. 6b, the entire impedance of cell-electrode interaction for the 3D graphene system can be expressed as (Equation 2)

$$Z_{cell-graphene} = R_{sol} + \frac{R_{seal}R_m}{R_m + R_{seal} + j\omega R_m R_{seal} C_m} + \frac{R_{ct}Z_{CPE1}}{R_{ct} + Z_{CPE1}} + \frac{R_L Z_{CPE2}}{R_L + R_{CPE2}} \quad (2).$$

It can be seen that because of the existence of quantum capacitance, the graphene interface has inherent structural advantages over the traditional gold interface in electrical impedance measurement.

Additionally, in order to estimate the cell capture efficiency of the designed microgrooves and the change of the electric field in microgrooves when cells were captured on the GMEAs, the finite element calculation software COMSOL 5.2a was used to simulate the distributions of flow rate and current density. In the flow rate simulation unit, the same hollow semi-cylindrical microgroove as the actual structure (Fig.1d) was adopted. The laminar flow was set to be 2 mm/s, and the diameter of the injection hole was assumed to be 1.5 mm. From the simulation result of velocity distribution, it can be seen that the flow velocity in the capture zone of microgrooves (not to exceed 1 mm/s) is much smaller than that in the side gap (greater than 5 mm/s) (Fig. 6d). Because the internal space of each microgroove can only accommodate single cell, and the difference in flow velocity between the capture zone and the external slit is considerable, the efficiency of single cell capture in the designed microgrooves could be 100 % (Nguyen et al., 2013). In the simulation unit of the electrostatic field, the interactions of single cell or two cells with the GMEAs were estimated. In particular, the breast cancer cells were equivalent to be spherical particles with a diameter of 20 μm, and the spacing between the working electrode and the reference electrode was set to be 120 μm. Other parameters including the conductivity and relative permittivity of materials and cells are displayed in Fig. 6(c) (Couniot et al., 2012). In this simulation, the middle of the cavity was filled with cell culture medium, while the cavities of

Accepted manuscript

both sides were filled with the single or double cells. The current density decreases significantly when the single cell or double cells is captured in the microgroove (Fig. 6e). As well as, the decreased current density of the microgrooves would translate into the enhanced impedance between the working electrode and the reference electrode, which is consistent with our experimental results.

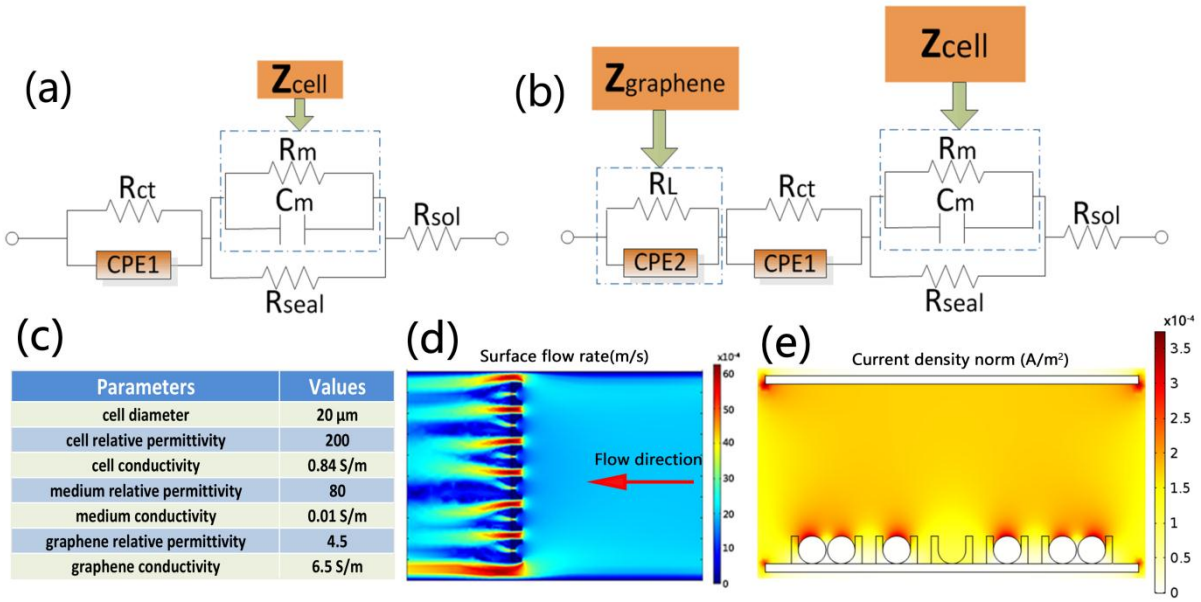

Parameters	Values
cell diameter	20 μm
cell relative permittivity	200
cell conductivity	0.84 S/m
medium relative permittivity	80
medium conductivity	0.01 S/m
graphene relative permittivity	4.5
graphene conductivity	6.5 S/m

Fig. 6.

5. Conclusions

Inspired by the topography and somatotype features of breast cancer cells, we have successfully prepared the 3D graphene biointerface that can be integrated on a microfluidic chip for cancer metastatic diagnosis and physiological behavior monitoring. Compared to classic 2D gold interface, the 3D graphene biointerface significantly improves the capture efficiency and sensing sensitivity of single cell, demonstrating the increment in impedance signal about 100% at the nodes of cell state change. These effects can be ascribed to the substantial increase in contact area and the significant improvement of topographical interaction between the cells and the graphene interface due to the matching of electrode

ACCEPTED MANUSCRIPT

structure and boundary dimension of cancer cell. The present work sheds new light on designing novel bio-inspired interfaces for dynamic study of cancer progression and clinical cell-related electrical signal analysis.

Acknowledgments

This work was supported by the National Natural Science Foundation of China (Nos. 51572242, 11372280 and 51502265), the Program for Changjiang Scholars and Innovative Research Team in University (No. IRT_17R98), the Zhejiang Provincial Natural Science Foundation of China (No. LY16E020011), the Program for Innovative Research Team of Zhejiang Sci-Tech University (No. 15010039-Y), and the Opening Fund of State Key Laboratory of Structural Analysis for Industrial Equipment of Dalian University of Technology (No. GZ1704).

Appendix A. Supporting information

Supplementary data associated with this article can be found in the online version at http://dx.doi.org/xxxxxxx.

References

Ang, P. K., Li, A., Jaiswal, M., Wang, Y., Hou, H. W., Thong, J. T., Lim, C. T., Loh, K. P., 2011. Nano. Lett. 11, 5240-5246.

Abdolahad, M., Taghinejad, M., Taghinejad, H., Janmaleki, M., Mohajerzadeh, S., 2012. Lab. Chip. 12, 1183-1190.

Abdolahad, M., Janmaleki, M., Taghinejad, M., Taghnejad, H., Salehi, F., Mohajerzadeh, S., 2013. Nanoscale 5, 3421-3427.

Accepted manuscript

ACCEPTED MANUSCRIPT

Abdolahad, M., Shashaani, H., Janmaleki, M., Mohajerzadeh, S., 2014. Biosens. Bioelectron. 59, 151-159.

Abiri, H., Abdolahad, M., Gharooni, M., Hosseini, S. A., Janmaleki, M., Azimi, S., Hosseini, M., Mohajerzadeh, S., 2015. Biosens. Bioelectron. 68, 577-585.

Borkholder, D. A, Stanford University, 1998.

Blau, A., 2013. Curr. Opin. Colloid. In. 18, 481-492.

Babahosseini, H., Srinivasaraghavan, V., Zhao, Z., Gillam, F., Childress, E., Strobl, J. S., Santos, W. L., Zhang, C., Agah, M., 2016. Lab. Chip. 16, 188-198.

Chang, B.-W., Chen, C.-H., Ding, S.-J., Chen, D. C.-H., Chang, H.-C., 2005. Sens. Actuators. B. Chem. 105, 159-163.

Couniot, N., Flandre, D., Francis, L., Afzalian, A., 2012. 26th European Conference on Solid–State Transducers, Eurosensor 47, 188-191.

Cai, P., Leow, W. R., Wang, X., Wu, Y. L., Chen, X., 2017. Adv. Mater. 29, 1605529.

Duy, L. T., Kim, D. J., Trung, T. Q., Dang, V. Q., Kim, B. Y., Moon, H. K., Lee, N. E., 2015. Adv. Funct. Mater. 25, 883-890.

Du, X., Wu, L., Cheng, J., Huang, S., Cai, Q., Jin, Q., Zhao, J., 2015. J Biol Phys 41, 339-347.

Ertel, A., Verghese, A., Byers, S. W., Ochs, M., Tozeren, A., 2006. Mol. Cancer. 5, 55-65.

Eyer, K., Stratz, S., Kuhn, P., Kuster, S., Dittrich, P., 2013. Anal. Chem. 85, 3280-3287.

Franks, W., Schenker, I., Schmutz, P., Hierlemann, A., 2005. IEEE. Trans. Biomed. Eng. 52, 1295-1302.

Fang, T., Konar, A., Xing, H., Jena, D., 2007. Appl. Phys. Lett. 91, 092109.

Feng, L., Wu, L., Qu, X., 2013. Adv. Mater. 25, 168-186.

Giaever, I., Keese, C. R., 1991. Proc. Natl. Acad. Sci. U. S. A. 88, 7896-7900.

Giaever, I., Keese, C. R., 1993. Nature 366, 591-592.

Accepted manuscript

ACCEPTED MANUSCRIPT

Guo, X. L., Zhu, R., 2016. Sci. Rep. 6, 31392-31397.

Han, A., Yang, L., Frazier, A. B., 2007.Clin. Cancer. Res. 13, 139-143.

Hong, J., Kandasamy, K., Marimuthu, M., Choi, C. S., Kim, S., 2011. Analyst 136, 237-245.

Hong, J. Y., Jang, J., 2012. J. Mater. Chem. 22, 8179-8191.

Hess, L. H., Jansen, M., Maybeck, V., Hauf, M. V., Seifert, M., Stutzmann, M., Sharp, I. D., Offenhausser, A., Garrido, J. A., 2011. Adv. Mater. 23, 5045-5049.

Hess, L. H., Seifert, M., Garrido, J. A., 2013. Proc. IEEE. Inst. Electr. Electron. Eng. 101, 1780-1792.

Jo, B.-H., Van Lerberghe, L. M., Motsegood, K. M.,Beebe, D. J., 2000. J. Microelectromech. S. 9, 76-81.

Keese, C. R., Wegener, J., Walker, S. R., Giaever, I., 2004. Proc. Natl. Acad. Sci. U. S. A. 101, 1554-1559.

Khademhosseini, A., Yeh, J., Eng, G., Karp, J., Kaji, H., Borenstein, J., Farokhzad, O. C., Langer, R., 2005. Lab. Chip. 5, 1380-1386.

Kim, W., Ng, J. K., Kunitake, M. E., Conklin, B. R., Yang, P., 2007. J. Am. Chem. Soc. 129, 7228-7229.

Keefer, E. W., Botterman, B. R., Romero, M. I., Rossi, A. F., Gross, G. W., 2008. Nat. Nanotechnol. 3, 434-439.

Kuzum, D., Takano, H., Shim, E., Reed, J. C., Juul, H.; Richardson, A. G., de Vries, J., Bink, H., Dichter, M. A., Lucas, T. H., Coulter, D. A., Cubukcu, E., Litt, B., 2014. Nat. Commun. 5, 5259-5268.

Levsky, J. M., Singer, R. H., 2003. Trends. Cell. Biol. 13, 4-6.

Liu, X., Chen, L., Liu, H., Yang, G., Zhang, P., Han, D., Wang, S., Jiang, L., 2013. NPG. Asia. Mater. 5, e63.

Liu, X. L., Wang, S. T., 2014. Chem. Soc. Rev. 43, 2385-2401.

Accepted manuscript

ACCEPTED MANUSCRIPT

Liu, Q., Wu, C., Cai, H., Hu, N., Zhou, J., Wang, P., 2014. Chem. Rev. 114, 6423-6461.

Li, Y., Lu, Q., Liu, H., Wang, J., Zhang, P., Liang, H., Jiang, L., Wang, S., 2015. Adv. Mater. 27, 6848-6854.

Liu, A. P., Zhao, L., Zhang, J. M., Lin, L. X., Wu, H. P., 2016. Acs. Appl. Mater. Inter. 8, 25210-25218.

Meadows, A. L., Kong, B., Berdichevsky, M., Roy, S., Rosiva, R., Blanch, H. W., Clark, D. S., 2008. Biotechnol. Prog. 24, 334-341.

Marcano, D. C., Kosynkin, D. V., Berlin, J. M., Sinitskii, A., Sun, Z. Z., Slesarev, A., Alemany, L. B., Lu, W., Tour, J. M., 2010. ACS Nano 4, 4806-4814.

Moodley, K., Angel, C. E., Glass, M., Graham, E. S., 2011. J. Neurosci. Meth. 200, 173-180.

Nikkhah, M., Edalat, F., Manoucheri, S., Khademhosseini, A., 2012. Biomaterials 33, 5230-5246.

Nguyen, T. A., Yin, T. I., Reyes, D., Urban, G. A., 2013. Anal. Chem. 85, 11068-11076.

Park, G.-S., Kwon, H., Kwak, D. W., Park, S. Y., Kim, M., Lee, J.-H., Han, H., Heo, S., Li, X. S., Lee, J. H., 2012. Nano. Lett. 12, 1638-1642.

Qian,W.Y., Zhang, Y., Chen, W.Q., 2015. Small 11, 3850-3872.

Robinson, J. T., Jorgolli, M., Shalek, A. K., Yoon, M.-H., Gertner, R. S., Park, H., 2012. Nat. Nanotechnol. 7, 180-184.

Solly, K., Wang, X., Xu, X., Strulovici, B., Zheng, W., 2004. Assay. Drug. Dev. Technol. 2, 363-372.

Sell, S., 2010. Am. J. Pathol. 176, 2584-2594.

Sun, T., Morgan, H., 2010. Microfluid. Nanofluids. 8, 423-443.

Sperber, M., Hupf, C., Lemberger, M.-M., Goricnik, B., Hinterreiter, N., Lukic, S., Oberleitner, M., Stolwijk, J. A., Wegener, J., 2015. Springer, pp 45-108.

Accepted manuscript

ACCEPTED MANUSCRIPT

Park, G.-S., Kwon, H., Kwak, D. W., Park, S. Y., Kim, M., Lee, J.-H., Han, H., Heo, S., Li, X. S., Lee, J. H., 2012. Nano. Lett. 12, 1638-1642.

Valastyan, S., Weinberg, R. A., 2011. Cell 147, 275-292.

Wang, K., Fishman, H. A., Dai, H., Harris, J. S., 2006. Nano. Lett. 6, 2043-2048.

Wang, L., Zhu, J., Deng, C., Xing, W.-l., Cheng, J., 2008. Lab. Chip. 8, 872-878.

Wu, H., Zhu, K., Cao, B., Zhang, Z., Wu, B., Liang, L., Chai, G., Liu, A., 2017. Soft Matter 13, 2995-3002.

Xiao, C., Lachance, B., Sunahara, G., Luong, J. H., 2002. Anal. Chem. 74, 1333-1339.

Xia, J., Chen, F., Li, J., Tao, N., 2009. Nat. Nanotechnol. 4, 505-509.

Xu, Y., Xie, X., Duan, Y., Wang, L., Cheng, Z., Cheng, J., 2016. Biosens. Bioelectron. 77, 824-836.

Yang, L., Li, Y., Fang, Y., 2013. Adv. Mater. 25, 3881-3887.

Zhao, L., Hong, C., Lin, L., Wu, H., Su, Y., Zhang, X., Liu, A., 2017. Carbon 116, 223-231.

Accepted manuscript

ACCEPTED MANUSCRIPT

Figure caption

Fig. 1. (a) 3D picture of designed microfluidic chip, which comprised three main parts, namely integrated electrode arrays, a PDMS channel with an inlet and an outlet and a PDMS lid. (b) Enlarged image of the capture area, including the corresponding position distribution of electrodes with different sizes. (c) Enlarged cross-section image of 3D graphene biointerface with an entrapped single cell. (d) Size of the 3D graphene modified photoresist-microgroove electrode for single cell capture.

Fig. 2. Production processes of 3D graphene modified microgrooves. (a) Substrate with PGEAs. (b) Negative photoresist spin-coating on the PGEAs. (c) UV exposure. (d) Development. (e) Enlarged image of photoresist-microgroove arrays on PGEAs substrate. The photoresist-microgroove arrays were treated with (f) O_2 plasma and (g) PDDA aqueous solution to make them hydrophilic. (h) GO solution was titrated onto the capture location of microfluidic channel. (i) GO was reduced under hydrazine hydrate vapor. (j) Single graphene modified microgroove was formed by the laser etching with a 0.8 J/cm^2 energy density.

Fig. 3. (a) Photograph of the microfluidic chip (2×2 cm^2). The integrated electrode arrays were connected to the corresponding visible large gold electrodes (2×2 mm^2) around the chip for the integration with PCB. (b) Magnified microscope image of microchannel with cell capture regions for single cell and double cells. (c) The height of hollow semicylinder was about 30 μm measured by using the laser microscope system. (d) Low-magnification and (e) high-magnification SEM images of microgroove arrays assembled with graphene sheets. (f) SEM image of the side wall of single graphene microgroove. (g) AFM image of the arc-shaped inside wall of graphene microgroove. (h) Optical microscope image of patterned graphene film after scanning with laser energy density of 0.8 J/cm^2. (i) 3D optical microscope picture of single capture unit after laser etching.

Accepted manuscript

ACCEPTED MANUSCRIPT

Fig. 4. Optical microscopy photographs of single cell and double cells captured at the corresponding microgroove interfaces. (a) Single and (b) double MCF-7 cells trapped in the microgrooves of 2D gold interfaces. (c) Single and (d) double MCF-7 cells trapped in the microgrooves of 3D graphene biointerfaces. Laser microscope images of (e) single and (f) double MCF-7 cells tightly enwrapped by the 3D graphene microgrooves. Laser microscope images of (g) single and (h) double MCF-7 cells squeezed by graphene microgrooves.

Fig. 5. Statistical analysis of the increment in impedance ΔZ at two frequencies of 5k Hz and 10k Hz. The data represented the mean of five results ± standard deviation (n=100). The ΔZ of (a) single MCF-7 cell or (b) single MDA-MB-231 cell seeding on the 2D gold interface and 3D graphene biointerface at different stages, including capture, attachment (incubate for 2h), spreading (incubate for 5h), and proliferation (incubate for 9h). The ΔZ of (c) double MCF-7 cells or (d) double MDA-MB-231 cells seeding on the 2D gold interface and 3D graphene biointerface at different stages.

Fig. 6. Electrical equivalent circuit models of (a) cell-gold interface interaction and (b) cell-graphene interface interaction. (c) Parameters used in the electric field simulation. (d) Simulation result of flow velocity distribution in channel. (e) Simulated current density distribution in capture location.

Accepted manuscript

Highlights

- Fabricate 3D graphene biointerface on the microfluidic chip
- A three-dimensional graphene biointerface for single-cell sensing
- Biointerface mimics the topography and somatotype features of cancer cells
- Improve cell-electrode interaction by contact area increase
- Monitor cancerous state and investigate cancer pathology

Graphical Abstracts

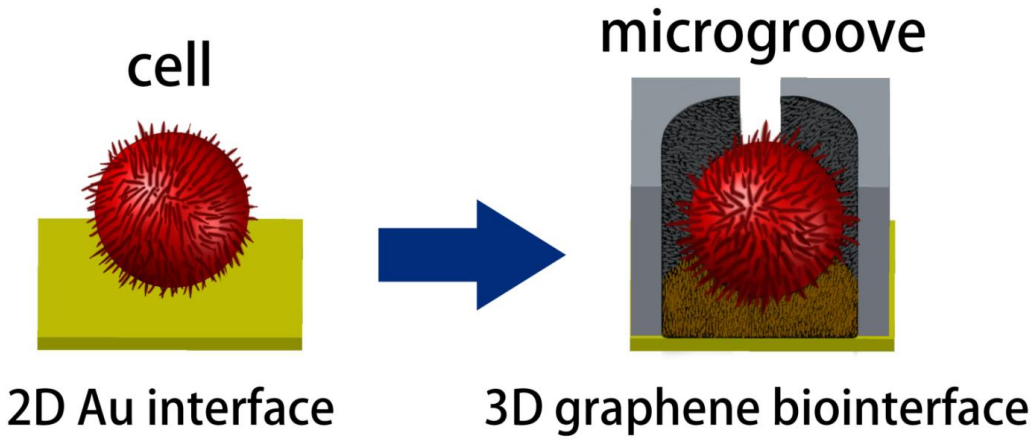

Accepted manus